Optical Engineering 49(5), 057004 (May 2010)

Image restoration and enhancement based on tunable forward-and-backward diffusion

Yi Wang
Ruiqing Niu
Xin Yu
China University of Geosciences
Institute of Geophysics and Geomatics
Lumo Road 388
Wuhan, Hubei 430074 China
E-mail: wangyi@whu.edu.cn

Liangpei Zhang
Wuhan University
State Key Laboratory of Information Engineering in Surveying, Mapping, and Remote Sensing
129 Luoyu Road
Wuhan, Hubei 430079 China

Huanfeng Shen
Wuhan University
School of Resource and Environmental Science
129 Luoyu Road
Wuhan, Hubei 430079 China

Abstract. In order to improve signal-to-noise ratio (SNR) and contrast-to-noise ratio, we introduces a novel tunable forward-and-backward (TFAB) diffusion approach for image restoration and edge enhancement. In the TFAB algorithm, an alternative forward-and-backward (FAB) diffusion process is presented, where it is possible to better modulate all aspects of the diffusion behavior and it shows better algorithm behavior compared to the existing FAB diffusion approaches. In addition, there is no necessity to laboriously determine the value of the gradient threshold. We believe the TFAB diffusion to be an adaptive mechanism for image restoration and enhancement. Qualitative experiments, based on various general digital images and a magnetic resonance image, show significant improvements when the TFAB diffusion algorithm is used versus the existing anisotropic diffusion and the previous FAB diffusion algorithms for enhancing edge features and improving image contrast. Quantitative analyses, based on peak SNR and the universal image quality index, confirm the superiority of the proposed algorithm. © *2010 Society of Photo-Optical Instrumentation Engineers.* [DOI: 10.1117/1.3431657]

Subject terms: anisotropic diffusion; forward and backward; tunable; image enhancement; image restoration.

Paper 090718R received Sep. 15, 2009; revised manuscript received Mar. 27, 2010; accepted for publication Apr. 6, 2010; published online Jun. 1, 2010.

1 Introduction

Digital images often suffer from a blurring effect and noise from various sources, such as different illumination conditions, image quantization, compression, transmission, etc. These sources of image degradation normally arise during image acquisition and processing and have a direct bearing on the visual quality of the image.[1] Undoing these imperfections to remove the image degradation is crucial for many image-processing tasks. Of particular interest to this study is the work related to image denoising and sharpening that aims to improve signal-to-noise ratio (SNR) and contrast-to-noise ratio (CNR).[2–7]

The scale-space concept was first presented by Iijima[8,9] and Weickert et al.[10] and became popular later on by the works of Witkin[11] and Koenderink.[12] The theory of linear scale-space supports edge detection and localization, while suppressing noise by tracking features across multiple scales.[11–16] In fact, the linear scale space can be expressed by a linear heat diffusion equation.[12,13] However, this equation was found to be problematic in that all edge features are smeared and distorted after a few iterations of linear diffusion. In order to remedy the difficulties encountered in the linear scale-space theory, Perona and Malik[17] developed an adaptive smoothing and edge-detectionscheme in which they replaced the linear heat diffusion equation by a selective diffusion that preserves edges. This development led some research to focus on the development of various anisotropic diffusion models and diverse numerical schemes to obtain steady-state solutions.[18–39] Among them, one specific anisotropic diffusion algorithm inspires us, the forward-and-backward (FAB) diffusion algorithm.[32]

In Perona and Malik's scheme,[17] the nonlinear diffusion process should be restricted by the "minimum-maximum" principle. This principle, to avoid creating any new minima or maxima, was obeyed by most nonlinear diffusion processes and guaranteed stability in partial differential equations (PDEs) and thus avoided the explosion of the nonlinear diffusion process. Instead of restricting the global extremes for the initial signal, Gilboa et al.[32] pointed out that inverse diffusion with a negative diffusion coefficient should be incorporated into image-sharpening and enhancement processes to deblur and enhance the extremes of the initial signal (if the extremes are indeed singularities and not generated by noise). However, linear inverse diffusion is a highly unstable process and results in noise amplification. Thus, nonlinear diffusion methods are further extended and combined with the FAB diffusion process to show that sharpening and denoising can be reconciled in image enhancement. Besides this pioneer work, some interesting work has been published on theoretical foundations and the application of FAB diffusion to gray and color images.[40–42]

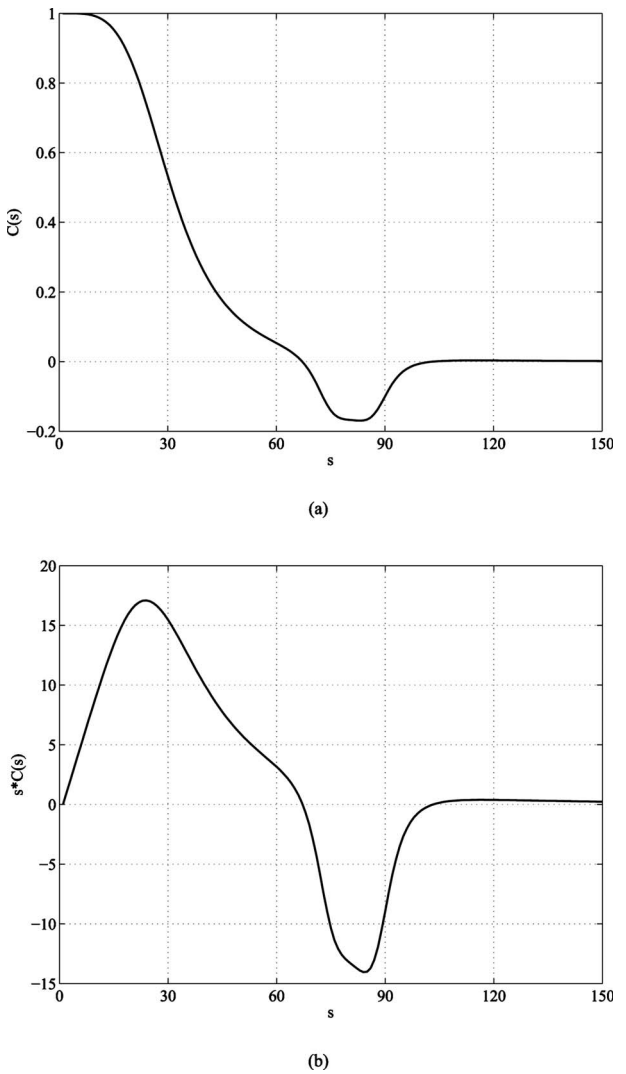

Fig. 1 The GSZ FAB diffusion coefficient Eq. (6) and the corresponding flux, plotted as a function of the gradient magnitude (k_f =30, k_b=80, w=10, α=0.25).

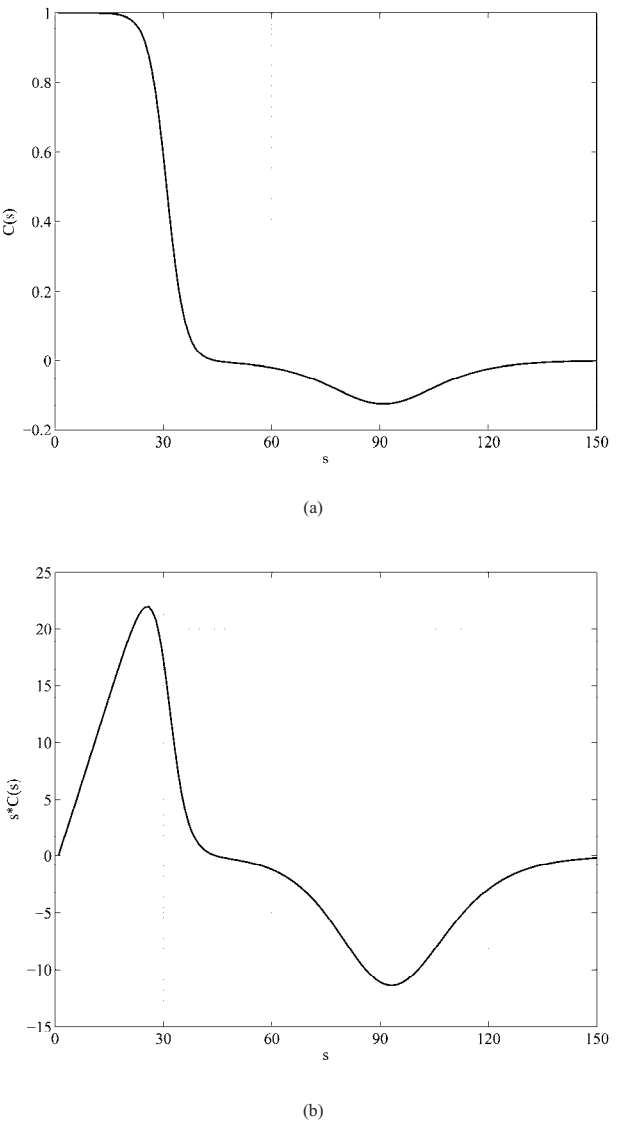

Fig. 2 The LVCFAB diffusion coefficient Eq. (7) and the corresponding flux, plotted as a function of the gradient magnitude (k_f=30, k_b =80, β_1=0.2, β_2=0.05, α=0.25).

In our earlier work,[39] we proposed a local variance-controlled forward-and-backward (LVCFAB) diffusion process in the context of image restoration and enhancement. In essence, this diffusion scheme is based on a better behaved diffusion coefficient, in which the transition length between the maximum and minimum values of diffusion coefficient does not increase with the gradient threshold. Although the scheme turns out to be effective for miscellaneous images, the location of the transition cannot be adjusted, which leads to difficulty in better controlling the diffusion behavior. Furthermore, it is yet uncovered about the optimal strategy for estimating the two gradient thresholds in the FAB diffusion scheme.

In this paper, we further develop our previous heuristic idea from an alternative perspective in order to come up with a systematic and tunable FAB diffusion algorithm. Unlike our earlier work, we explore an alternative FAB diffusion process based on a suitable sigmoid function, in which both the location of the transition from isotropic to oriented flux and the transition length can be easily tuned. As a result, our tunable FAB (TFAB) algorithm is more effective at controlling the behavior of the diffusion function when compared to the existing FAB diffusion approaches. In addition, it is not necessary to determine the value of the gradient because since there is no such parameter in the diffusion coefficient. We believe the alternative FAB diffusion algorithm to be a novel mechanism for image restoration and enhancement.

The remainder of this paper is organized as follows: Section 2 presents the proposed TFAB diffusion algorithm; Section 3 describes simulations including comparative results between several existing anisotropic diffusion schemes and our proposed algorithm; and Section 4 states our concluding remarks.

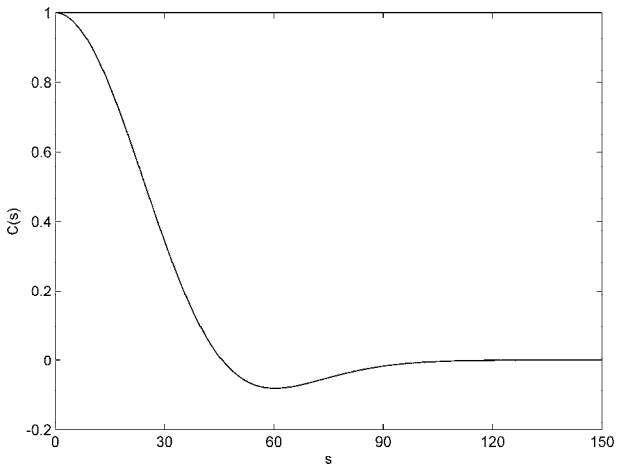

(a)

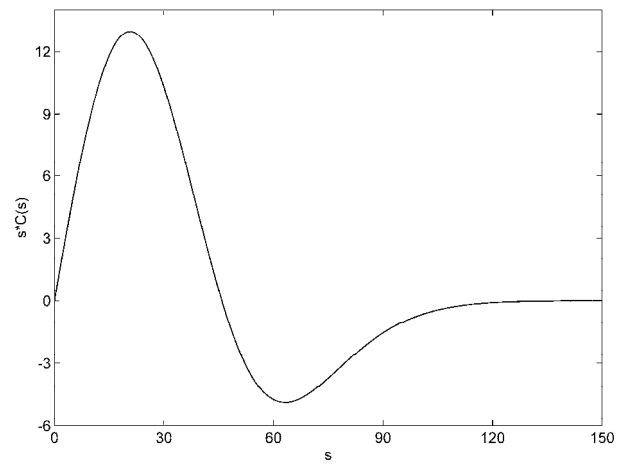

(b)

Fig. 3 Diffusion coefficient Eq. (8) and the corresponding flux, plotted as a function of the gradient magnitude ($\beta=5\times10^{-4}$, $\gamma=10$, $\xi=2$).

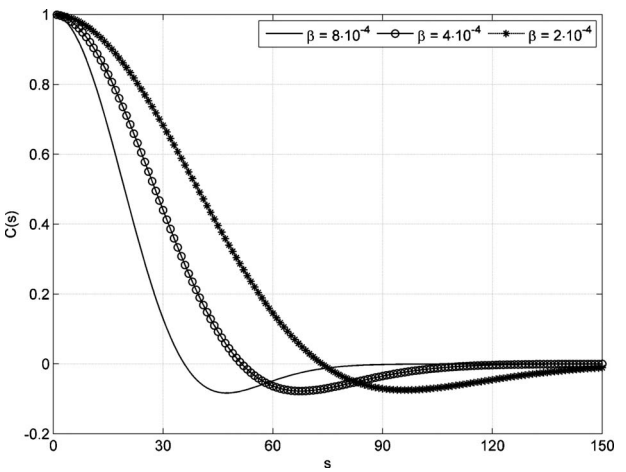

Fig. 4 Tunable diffusion coefficients with the different parameter β ($\gamma=10$, $\xi=2$).

$$E(I)=\int_{\Omega}|\hat{I}-I_0|^2dx+\lambda\cdot\int_{\Omega}\phi(|\nabla I|)dx, \tag{2}$$

where Ω is the image domain and $\hat{I}=LI$. The first term on the right-hand side of Eq. (2) is the quadratic data fidelity term, and the second term represents a prior assumption about the true image I. Selecting a suitable regularizer ϕ is paramount in restoring/enhancing the edges and is an open problem. Nonconvex regularizing functions have also been used in the past[17,43–45] in spite of the absence of existence results. The equivalence of these methods to the anisotropic PDE-based models can be seen via the Euler–Lagrange equation. Starting with the pioneering work of

2 TFAB Diffusion Algorithm

2.1 *FAB Diffusion*

In image restoration, the problem of finding the true image is modeled as follows:[43]

$$I_0=\hat{I}+n, \tag{1}$$

where I_0 is the noisy output result of this linear model that is given to us. $\hat{I}=LI$ is a blurred version of the original image I, L is a linear operator representing the blur, usually a convolution. The additive noise is given by n with the assumed known mean and variance σ^2. This, in general, is an ill-posed problem. Edge-preserving regularization methods are proposed to restore the image,[43,44] by minimizing the following energy functional:

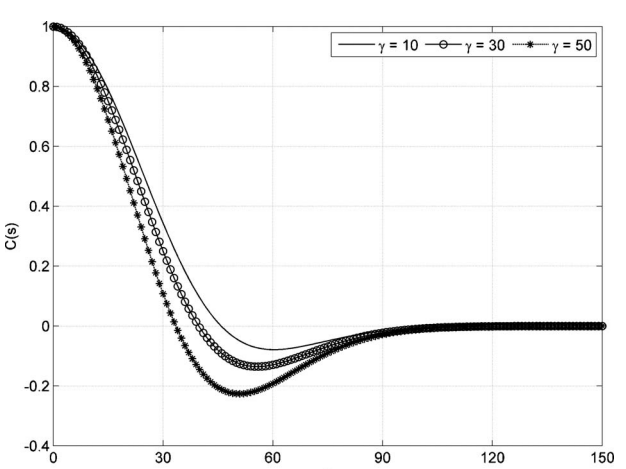

Fig. 5 Tunable diffusion coefficients with the different parameter γ ($\beta=5\times10^{-4}$, $\xi=2$).

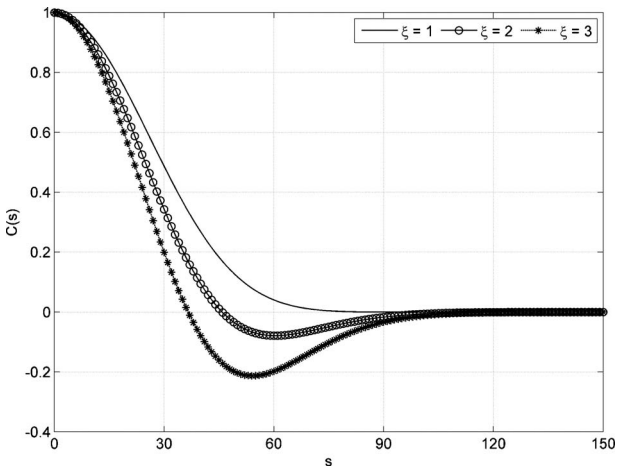

Fig. 6 Tunable diffusion coefficients with the different parameter ξ ($\beta=5\times10^{-4}$, $\gamma=10$).

Perona–Malik,[17] the following class of second-order PDEs are used extensively used in image restoration and in other early vision problems:

$$\frac{\partial I(x,y,t)}{\partial t} = \mathrm{div}\{c[\nabla I(x,y,t)]\,\nabla\, I(x,y,t)\}, \tag{3}$$

where ∇ is the gradient operator and div is the divergence operator. $c(\cdot)$ is a non-negative monotonically decreasing function of local spatial gradient. If $c(\cdot)$ is constant, then isotropic diffusion is enacted. In this case, all locations in the image, including the edges, are equally smoothed. This

Fig. 7 Enhanced images for Parrots image: (a) Original image with 8-bit gray levels; (b) Gaussianly blurred Lena image ($\sigma=1$), contaminated by zero-mean Gaussian noise with 50; (c) CLMC anisotropic diffusion ($\rho=0.05$); (d) MB anisotropic diffusion ($\rho=0.05$); (e) GSZ FAB diffusion ($k_f=0.2*\mathrm{MAG}$, $k_b=0.4*\mathrm{MAG}$, $\alpha=0.2$); (f) LVCFAB diffusion ($k_f=50$, $k_b=200$, $\beta_1=0.2$, $\beta_2=0.02$, $\rho=0.2$, $\alpha=0.2$); and (g) TFAB diffusion ($\beta=0.006$, $\gamma=3$, $\xi=2$) (15 iterations).

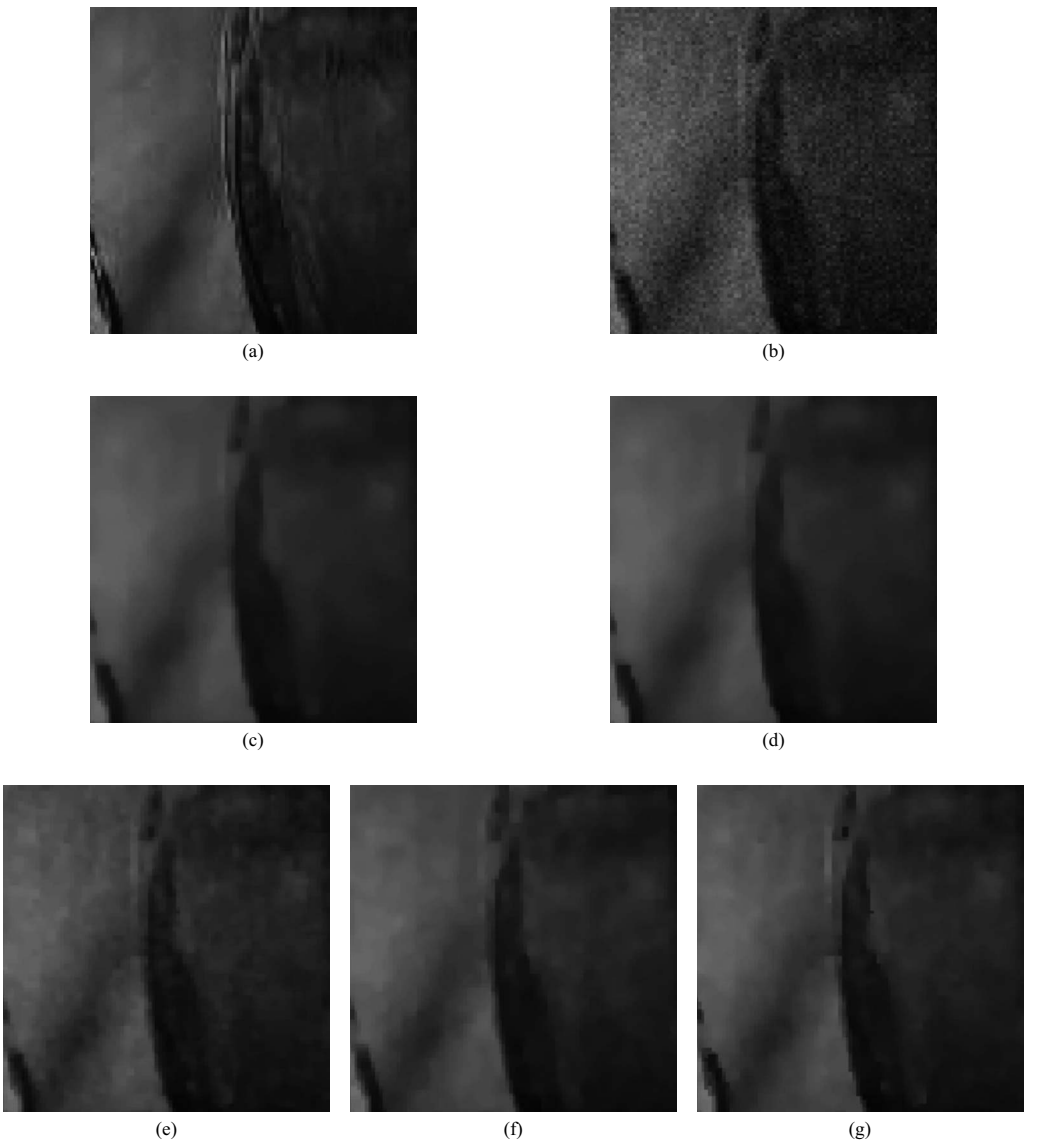

Fig. 8 A regional enlarged portion of homogeneous zones of original noise-free image, blurred and noisy image, and results corresponding to Fig. 7(c)–7(g).

is an undesirable effect because the process cannot maintain the natural boundaries of objects. One common form of $c(\cdot)$ is

$$c[\nabla I(x,y,t)] = \frac{1}{1+[\|\nabla I(x,y,t)\|/k]^{1+\alpha}}, \quad \text{where } \alpha > 0, \qquad (4)$$

where the parameter k serves as a gradient threshold: a smaller gradient is diffused and positions of a larger gradient are treated as edges.

The diffusion coefficient (4) is chosen to be nonincreasing functions of the image gradient. This scheme selectively smoothes regions without large gradients. However, in the FAB diffusion process, the points of extremes are emphasized in signal enhancement, image sharpening, and restoration. The emphasized extremes occur if these points are indeed represented by singularities and do not emerge as the result of noise. It was observed by Gilboa et al. that if we want to emphasize large gradients we should like to move "mass" from the lower part of a "slope" upwards.[32] This process can be viewed as "moving back in time" along the scale space, or reversing the diffusion process. Mathematically, this can be accomplished simply by changing the sign of the diffusion coefficient

$$\frac{\partial I(x,y,t)}{\partial t} = \mathrm{div}\{-c[\nabla I(x,y,t)]\,\nabla I(x,y,t)\}. \qquad (5)$$

However, we cannot simply use an inverse anisotropic diffusion process for image enhancement because it is highly unstable. There is a major problem associated with the backward diffusion: noise amplification. To remedy this

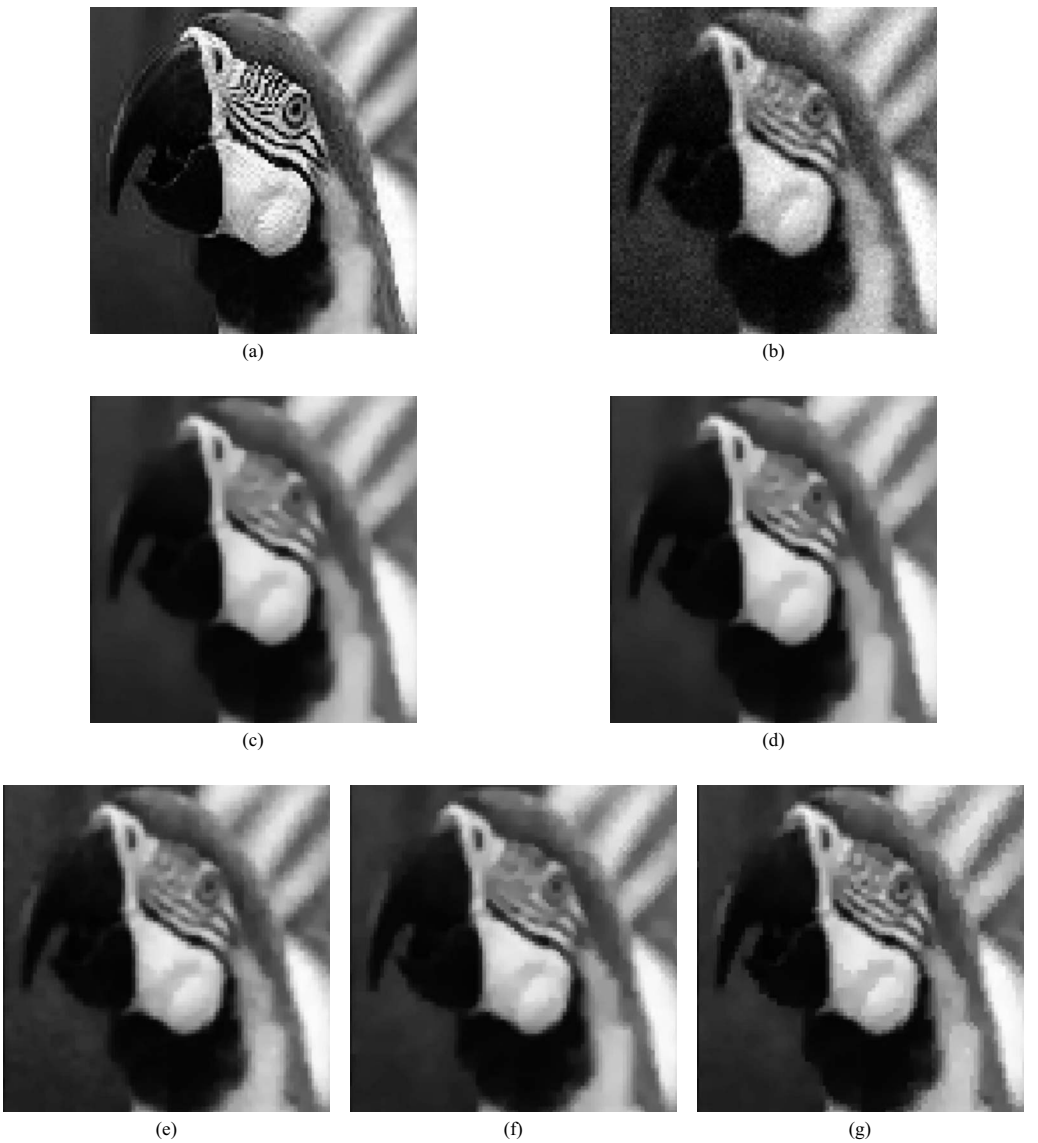

Fig. 9 Regional enlarged portion of edge features of original noise-free image, blurred and noisy image, and results corresponding to Fig. 7(c)–7(g).

drawback of the linear inverse diffusion process, Gilboa et al.[32] proposed that two forces of diffusion working simultaneously on the signal are needed. First, a backward force is used at medium gradients, where singularities are expected, and the second, a forward force, is implemented for suppressing oscillations and reducing noise. The forward and backward forces are combined into one coupled FAB diffusion process with a diffusion coefficient that possesses both positive and negative values. Thus, a diffusion coefficient (see Fig. 1) that controls the Gilboa–Sochen–Zeevi (GSZ) FAB diffusion process was proposed[32]

$$c[\nabla I(x,y,t)] = \frac{1}{1+[\|\nabla I(x,y,t)\|/k_{\mathrm{f}}]^n} - \frac{\alpha}{1+\{[\|\nabla I(x,y,t)\|-k_{\mathrm{b}}]/w\}^{2m}}, \tag{6}$$

where k_{f} is similar to the role of the parameter k in the PM diffusion equation; k_{b} and w define the range of backward diffusion, and are determined by the value of the gradient that is emphasized; α controls the ratio between the forward and backward diffusion; and the exponent parameters (n,m) are chosen as $(n=4,\ m=1)$. Equation (6) is locally adjusted according to image features, such as edges, textures, and moments. The GSZ FAB diffusion process can therefore enhance features while locally denoising the smoother segments of images.

However, the transition length between the maximum and minimum coefficient values varies with the gradient threshold, which makes controlling the evolution procedure

Fig. 10 Enhanced images for Couple image: (a) Original image with 8-bit gray levels; (b) Gaussianly blurred image (σ=1), contaminated by zero-mean Gaussian noise with 50; (c) CLMC anisotropic diffusion (ρ=0.05); (d) MB anisotropic diffusion (ρ=0.05); (e) GSZ FAB diffusion (k_f=0.2∗MAG, k_b=0.4∗MAG, α=0.2); (f) LVCFAB diffusion (k_f=50, k_b=200, β_1=0.2, β_2=0.02, ρ=0.2, α=0.2); and (g) TFAB diffusion (β=0.006, γ=8, ξ=2) (15 iterations).

difficult.[39] Thus, we proposed the LVCFAB diffusion coefficient (see Fig. 2) as follows:[39]

$$c[\nabla I(x,y,t)] = \frac{1-\tanh\{\beta_1 \cdot [\|\nabla I(x,y,t)\| - k_f]\} - \alpha \cdot (1-\tanh^2\{\beta_2 \cdot [k_b - \|\nabla I(x,y,t)\|]\})}{2}, \tag{7}$$

where β_1 and β_2 control the steepness for the min-max transition region of forward diffusion and backward diffusion, respectively. These two parameters are vital to the FAB diffusion behavior, and the transition width from iso-

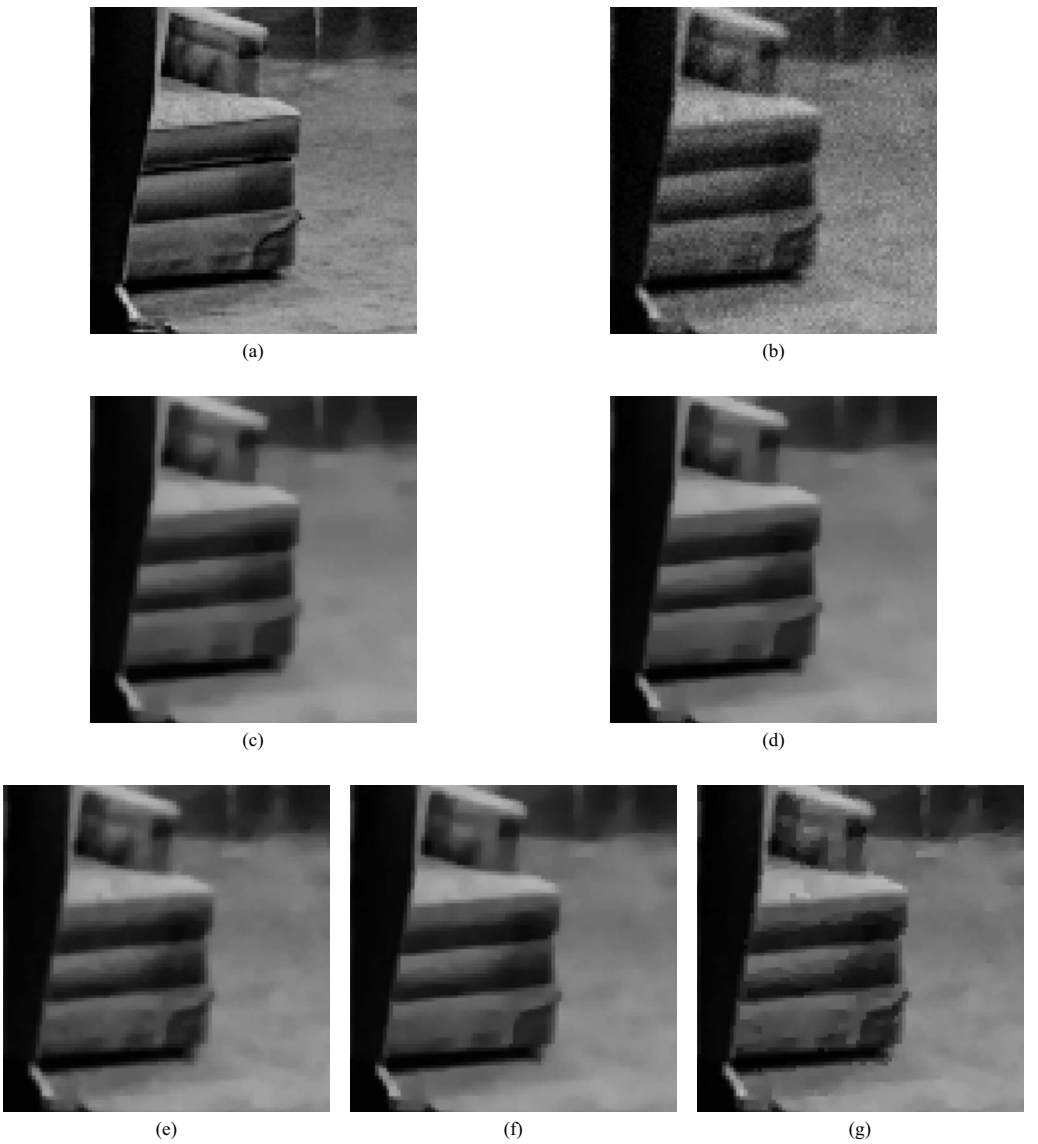

Fig. 11 Regional enlarged portion of interest of original noise-free image, blurred and noisy image, and results corresponding to Fig. 10(c)–10(g).

tropic to oriented flux can be altered by modulating them. In addition, the LVCFAB diffusion process can preserve the transition length from isotropic to oriented flux and, thus, it is better at controlling the diffusion behavior than that of the GSZ FAB diffusion.

2.2 *Alternative FAB (AFAB) Diffusion*

In this section, an AFAB diffusion is presented to be able to modulate everything: the location of the transition from isotropic to oriented diffusion and the corresponding transition length. In this paper, we define an AFAB diffusion coefficient (see Fig. 3) that is based on a suitable sigmoid function as follows:

$$c[\nabla I(x,y,t)] = \frac{e^{-\beta\gamma^2} + e^{-\beta[\|\nabla I(x,y,t)\|]^2} + \xi \cdot (e^{-\beta[\|\nabla I(x,y,t)\|]^2} - 1)}{e^{-\beta\gamma^2} + e^{\beta[\|\nabla I(x,y,t)\|]^2}}, \tag{8}$$

where β denotes the length of transition from isotropic to oriented flux, γ governs the transition location of FAB diffusion, and ξ dominates the transition coefficient. Figs. 1–3 show plots of the diffusion coefficients and respective

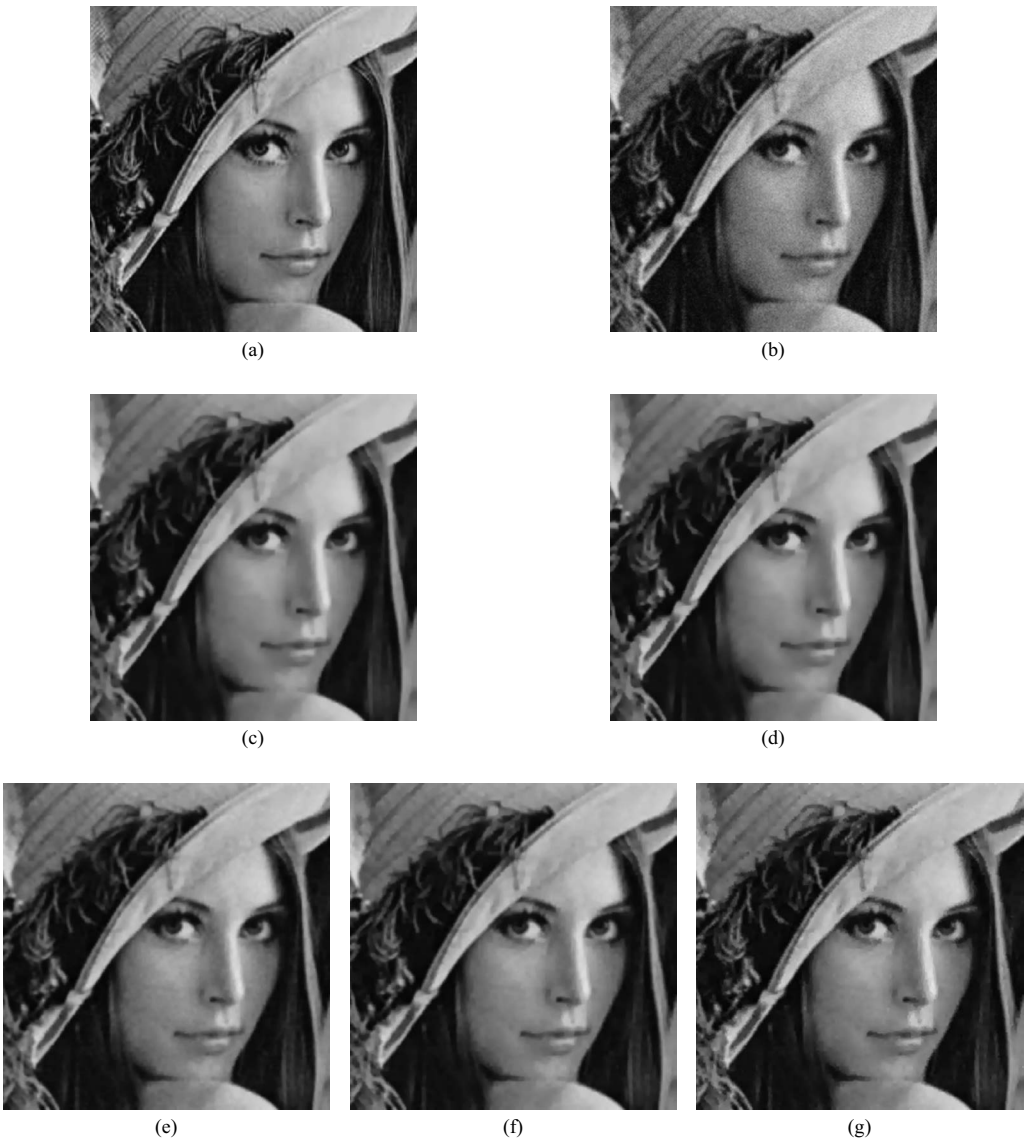

Fig. 12 Enhanced images for Lena image: (a) Original image with 8-bit gray levels. (b) Gaussianly blurred Lena image ($\sigma=1$), contaminated by zero-mean Gaussian noise with 50; (c) CLMC anisotropic diffusion ($\rho=0.05$); (d) MB anisotropic diffusion ($\rho=0.05$); (e) GSZ FAB diffusion ($k_f=0.2*\mathrm{MAG}$, $k_b=0.4*\mathrm{MAG}$, $\alpha=0.2$); (f) LVCFAB diffusion ($k_f=50$, $k_b=200$, $\beta_1=0.2$, $\beta_2=0.04$, $\rho=0.2$, $\alpha=0.2$); and (g) TFAB diffusion ($\beta=0.006$, $\gamma=8$, $\xi=2$) (15 iterations).

fluxes of the threeFAB diffusion coefficients. It is apparent that the proposed diffusion coefficient has a different formulation to that of the GSZ FAB and LVCFAB diffusion coefficients. However, they all combine two opposing forces into the diffusion process: one backward force at medium gradients for sharpening, and a second, a forward force at low gradients for smoothing and restoration. Furthermore, they have the same property: negative diffusion coefficients are explicitly employed in a certain gradient range. Meanwhile, there is no gradient threshold k in Eq. (8), are used which is helpful in reducing the complexity of the parameter selection procedure.

2.3 *Parameter Analysis*

To better control the diffusion coefficient, we analyze the effect of varying the different parameters and show how the tunability is related to diffusion behavior. From Figs. 1–3, we observe remarkably that the plot of the FAB diffusion coefficient will always drop and rise to zero, so that smoothing is performed when the diffusivity function is positive and sharpening occurs for negative diffusion coefficient values. In Eq. (8), γ determines the location of this drop and rise occurs. As γ increases, the drop part of the location will descend, while the rise part will ascend

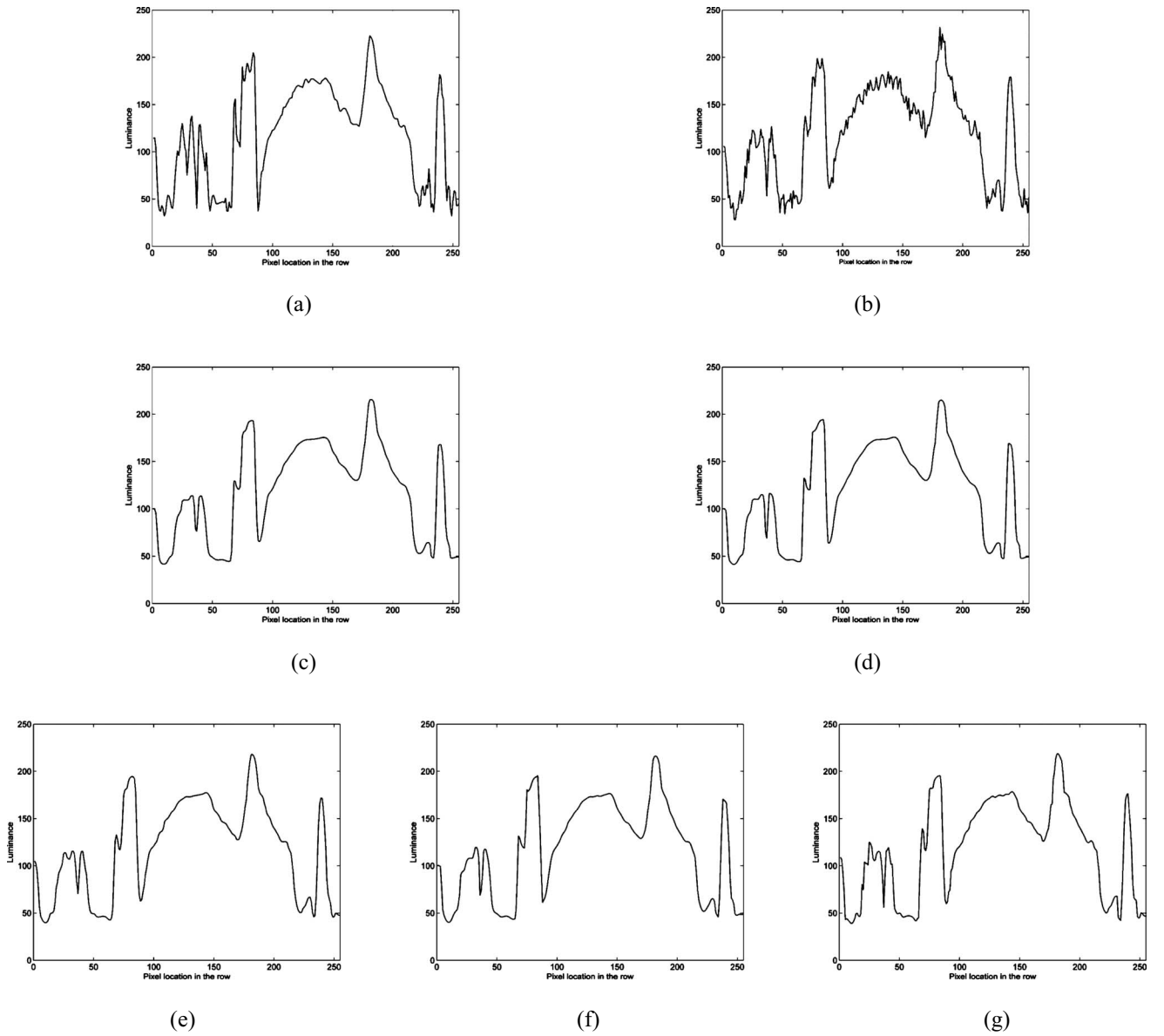

Fig. 13 Intensity values of row 138: (a) in the original Lena image, (b) in the blurred and noisy image, and in the results given by (c) CLMC anisotropic diffusion, (d) MB anisotropic diffusion, (e) GSZ FAB diffusion, (f) LVCFAB diffusion, and (g) TFAB diffusion.

(see Fig. 4). This rule is helpful for setting the proper value of γ to control the location of the transition from isotropic to oriented flux. Meanwhile, both the GSZ FAB and LVCFAB diffusion coefficients have a given transition location and, therefore are not adjustable. The function curves of the proposed FAB diffusion coefficient with different β values are depicted in Fig. 5. It is noted that β is closely related to how fast the drop happens. Moreover, the plot of the diffusion coefficient in Fig. 5 declines faster as β increases. Obviously, β is a crucial parameter that can offer much flexibility to achieve specific FAB diffusion characteristics. In our previous work, we employed the two similar parameters to the LVCFAB diffusion process to control the shape of the diffusion function where the diffusion coefficient is positive and negative. However, the GSZ FAB scheme has no such variables.[39] ξ can be used to control the ratio between the FAB diffusion. It can be observed from Fig. 6 that if $\xi > 1$, then the diffusion scheme with the diffusion coefficient (8) serves as a tunable FAB diffusion process. On the contrary, if $\xi \leqslant 1$, then the proposed diffusion scheme transforms to the traditional anisotropic diffusion process, where the diffusion coefficient is always positive.

2.4 *TFAB Diffusion Algorithm*

In this section, we summarize the idea of the TFAB diffusion coefficient mentioned above into a complete and adaptive image-restoration and -enhancement algorithm. To achieve this goal, we propose to filter the data by the following algorithm of FAB diffusion.

1. Initialization

   a. Input a given image I. $I(x,y,0)$ denotes the original intensity of pixel (x,y).

   b. Set parameters β, γ, and ξ for the proposed FAB diffusion; and T for the maximal number of iterations.

2. Iterate until $t=T$.

   a. For each pixel (x,y), the diffusion coefficient $c[\nabla I(x,y,t)]$ is computed by Eq. (8).

   b. The four-nearest-neighbor diffusion discretization equation is performed to update $I(x,y,t)$. Our FAB diffusion algorithm is a discretization on a 3×3 lattice. In order to accomplish the assumptions mentioned above, we propose the following anisotropic diffusion equation:

$$I(x,y,t+1) = I(x,y,t) + \lambda \cdot (c_N \cdot \nabla_N I + c_S \cdot \nabla_S I + c_E \cdot \nabla_E I + c_W \cdot \nabla_W I),$$

   where N, S, E, and W are the mnemonic subscripts for four directions (i.e., North, South, East, and West). The subscripts on the parenthesis are applied to all the terms enclosed. λ is the time step: $0 \leqslant \lambda \leqslant 1/4$ for the numerical scheme to be stable. As defined in the original paper,[46] the spatial gradient at pixel (x,y) is the first derivative of its image intensity function.

3 Experiments

In this section, we first describe the methodology used in our simulations and then reveal comparative filtering results for blurred and noisy images. Moreover, we provided detail discussion on the impact of parameters and the performance of the proposed algorithm at different noise levels. Finally, we demonstrate that as a useful tool for early vision, the proposed algorithm effectively extracts fine edge structures from medical images.

In order to demonstrate the effectiveness, we compare our algorithm to two traditional anisotropic diffusion algorithms: Catte-Lions-Morel-Coll (CLMC) anisotropic diffusion[18] and Monteil-Beghdadi (MB) anisotropic diffusion.[47] We also apply two existing FAB diffusion algorithms: GSZ FAB diffusion[32] and LVCFAB diffusion.[39] The ultimate goal of image filtering is to facilitate the subsequent processing for computer vision. To demonstrate the validity of the proposed algorithm in an early vision task, we apply the above diffusion algorithms to enhance a medical image for an application-based evaluation. As a defining characteristic, iterative operations are inevitably involved in anisotropic diffusion. Therefore, implementation of an iterative algorithm depends greatly on the termination time, which causes what we often refer to as the termination problem. Although there still does not exist a widely accepted analytical method, several heuristic methods have been proposed to determine the stopping time to overcome instability in anisotropic diffusion.[26,40,48,49] As far as simplicity is concerned, the nonlinear cooling method is most suitable for applications as a general denoising scheme. Gilboa et al.[48] proposed a threshold-freezing nonlinear cooling method, using the cooling rate we refer to as ρ, and applied it to the anisotropic diffusion scheme. In our simulations, we adopted this strategy in the CLMC and MB anisotropic diffusion and GSZ FAB diffusion. Meanwhile, the gradient threshold of the GSZ FAB diffusion is determined by calculating the mean absolute gradient (MAG) from the original paper.[32]

Table 1 PSNR and quality value for images of Parrots, Lena, Cameraman, and Couple.

Scheme	Image	PSNR (dB)	UIQI
Blurred and noisy	Parrots	27.07	0.5351
	Lena	34.98	0.6910
	Cameraman	25.29	0.4066
	Couple	26.97	0.6866
CLMC	Parrots	28.17	0.7313
	Lena	35.70	0.7646
	Cameraman	25.66	0.4690
	Couple	27.55	0.6934
MB	Parrots	28.27	0.7303
	Lena	35.88	0.7638
	Cameraman	25.77	0.4763
	Couple	27.62	0.6955
GSZ FAB	Parrots	28.37	0.7348
	Lena	36.43	0.8174
	Cameraman	25.89	0.5100
	Couple	27.81	0.7391
LVCFAB	Parrots	28.35	0.7462
	Lena	36.42	0.8142
	Cameraman	25.93	0.5017
	Couple	27.90	0.7239
TFAB	Parrots	28.42	0.7514
	Lena	36.72	0.8214
	Cameraman	25.97	0.5224
	Couple	27.97	0.7556

(a) $\beta = 0.002$

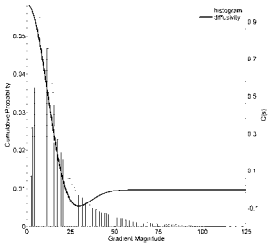

(b) The histogram of the original Lena image and diffusivity ($\beta = 0.002$)

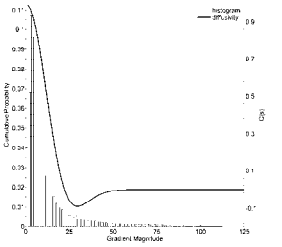

(c) The histogram of the filtered Lena image and diffusivity ($\beta = 0.002$)

(d) $\beta = 0.004$

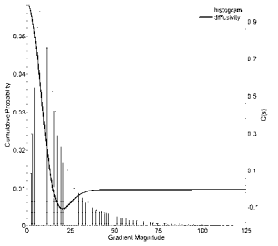

(e) The histogram of the original Lena image and diffusivity ($\beta = 0.004$)

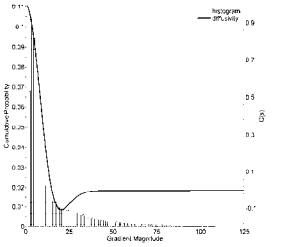

(f) The histogram of the filtered Lena image and diffusivity ($\beta = 0.004$)

(g) $\beta = 0.006$

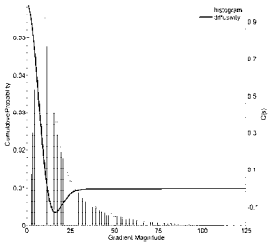

(h) The histogram of the original Lena image and diffusivity ($\beta = 0.006$)

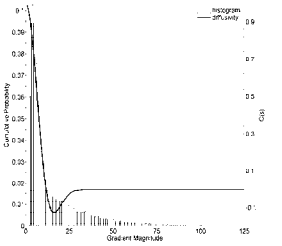

(i) The histogram of the filtered Lena image and diffusivity ($\beta = 0.006$)

(j) $\beta = 0.008$

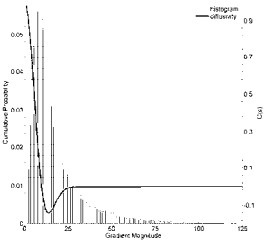

(k) The histogram of the original Lena image and diffusivity ($\beta = 0.008$)

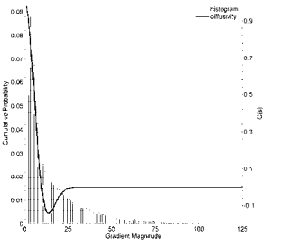

(l) The histogram of the filtered Lena image and diffusivity ($\beta = 0.008$)

(m) $\beta = 0.01$

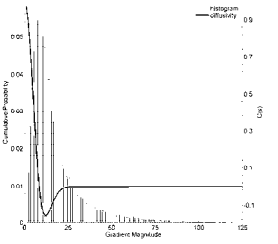

(n) The histogram of the original Lena image and diffusivity ($\beta = 0.01$)

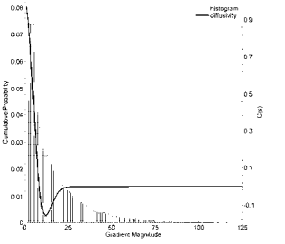

(o) The histogram of the filtered Lena image and diffusivity ($\beta = 0.01$)

Fig. 14 Impact of β on the TFAB diffusion method's performance (γ=8, ξ=2).

Table 2 PSNR and quality value for Lena image with different γ.

Parameter	PSNR (dB)	UIQI
$\gamma=1$	36.73	0.8174
$\gamma=4$	36.79	0.8192
$\gamma=9$	36.72	0.8203
$\gamma=16$	36.05	0.7967
$\gamma=25$	35.18	0.7507

Table 3 PSNR and quality value for Lena image with different β.

Parameter	PSNR (dB)	UIQI
$\beta=0.002$	35.89	0.7809
$\beta=0.004$	36.57	0.8076
$\beta=0.006$	36.72	0.8214
$\beta=0.008$	36.70	0.8126
$\beta=0.01$	36.38	0.7955

3.1 *General Images*

The performance of the proposed algorithm is evaluated using four 256×256 standard images with 256 gray-scale values. The image of Parrots is used as an example of the piecewise-constant image. Lena and Cameraman are two examples with both textures and smooth regions. Couple is an example with different edge features. Figure 7(a) shows the original noise-free Parrots image. For the test, we generate a blurred and noisy version of the image, as shown in Fig. 7(b). The results yielded by CLMC and MB anisotropic diffusion are depicted in Figs. 7(c) and 7(d), respectively. We can observe that the two algorithms result in the loss of important information from the original image, though the noise is entirely removed. A better combination of smoothing and sharpening is given by the GSZ FAB and LVCFAB diffusion processes. Figs. 7(e) and 7(f) show the corresponding results. Finally, the image yielded by our algorithm is represented in Fig. 7(g). The noise is readily removed, and this is due to tunable forward diffusion. Meanwhile, edge features, including most of the fine details, are sharply reproduced with the TFAB diffusion algorithm. From the perspective of vision quality, the results given by the GSZ FAB, the LVCFAB, and the TFAB diffusion are comparable because the three processes simultaneously enhance, sharpen, and denoise images. Nevertheless, the degree of enhancement of the TFAB diffusion could be tuned more appropriately to account for improving the SNR and CNR.

In order to obtain a better evaluation of the visual quality of the enhanced images, two regional enlarged portions of interest in Fig. 7 [see Fig. 7(a)], and the corresponding enhanced results are zoomed in Figs. 8 and 9. From these details, we can easily observe that all the diffusion algorithms mentioned above could reduce noise. Nevertheless, the CLMC and MB anisotropic diffusion algorithms blur significant edge features. The homogeneous zones and edge features processed by the GSZ FAB, LVCFAB, and TFAB diffusion algorithms are depicted in Figs. 8(e)–8(g) and 9(e)–9(g), respectively. It is quite obvious that the GSZ FAB and LVCFAB diffusion algorithms achieve a good compromise between sharpening and denoising, while the proposed algorithm exhibits the best edge-enhanced diffusion behavior [for a comparison, see the original portions in Figs. 8(a) and 9(a), respectively].

Figure 10(a) shows the image of Couple. Figure 10(b) is the blurred and noisy version of Fig. 10(a), generated by adding Gaussian blur and noise. We apply five diffusion algorithms to the blurred and noisy image and illustrate resulting images in Figs. 10(c)–10(g). In order to have a clearer view, one region of interest in Fig. 10 is displayed in Fig. 11 for the five algorithms. It can be seen that noise is thoroughly removed in the enhanced images; however, many important features are missing or blurred with the CLMC and MB anisotropic diffusion algorithms used for comparison. In contrast, our algorithm delivers the best visual quality among the three FAB diffusion algorithms; most fine details are enhanced well during the evolutionary process.

We also present in Fig. 12 the image of Lena to show the effects of the five diffusion algorithms applied in this study. The resulting images are presented in Figs. 12(c)–12(g). It is observed that the TFAB diffusion produces the best image, judged by subjective image quality, compared to the other four algorithms. In order to appraise the nonlinear behavior of the five anisotropic diffusion algorithms, the intensity values of a row are graphically depicted in Fig. 13. The original noise-free row number 138 (from top to bottom) is shown in Fig. 13(a). The corresponding row in the blurred and noisy image is represented in Fig. 13(b). According to the previous observation, the CLMC and MB anisotropic diffusion algorithms blur significant edge features and the results are shown in Figs. 13(c) and 13(d). The data processed by the GSZ FAB, LVCFAB, and TFAB diffusion algorithms are depicted in Figs. 13(e)–13(g), respectively. It is obvious that the GSZ FAB and LVCFAB diffusion algorithms can reconcile the balance between sharpening and denoising, while the proposed algorithm exhibits the best edge-enhanced diffusion behavior [for a comparison, see the original image in Fig. 13(a)]. It is evident from the comparative results that our algorithm outperforms the others in terms of sharpening and restoration of the blurred and noisy image.

In order to objectively evaluate the performance of the different diffusion algorithms, we adopt the peak SNR (PSNR) and universal image quality index (UIQI). The PSNR is used to estimate the effectiveness of noise reduction:

$$\mathrm{PSNR}=10\log_{10}\left(\frac{\sum_{i,j}255^2}{\sum_{i,j}[I(i,j,0)-I(i,j,T)]^2}\right)\mathrm{dB}, \tag{9}$$

where $I(0)$ is the original image and $I(T)$ denotes the recovered image. Recently, UIQI has been widely used to better evaluate image quality[50]

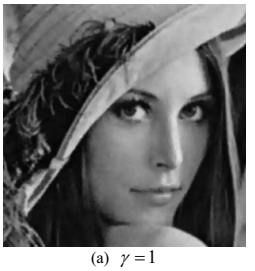

(a) $\gamma = 1$

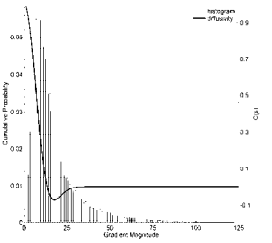

(b) The histogram of the original Lena image and diffusivity ($\gamma = 1$)

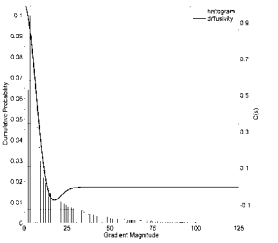

(c) The histogram of the filtered Lena image and diffusivity ($\gamma = 1$)

(d) $\gamma = 4$

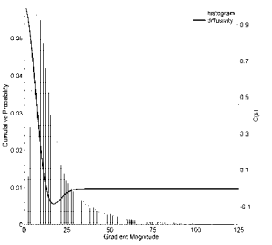

(e) The histogram of the original Lena image and diffusivity ($\gamma = 4$)

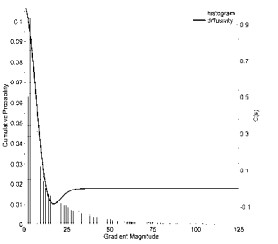

(f) The histogram of the filtered Lena image and diffusivity ($\gamma = 4$)

(g) $\gamma = 9$

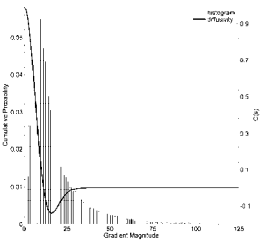

(h) The histogram of the original Lena image and diffusivity ($\gamma = 9$)

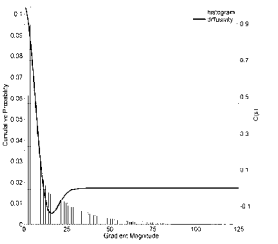

(i) The histogram of the filtered Lena image and diffusivity ($\gamma = 9$)

(j) $\gamma = 16$

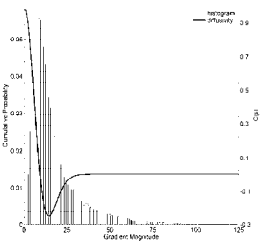

(k) The histogram of the original Lena image and diffusivity ($\gamma = 16$)

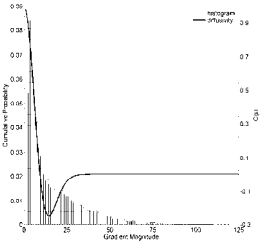

(l) The histogram of the filtered Lena image and diffusivity ($\gamma = 16$)

(m) $\gamma = 25$

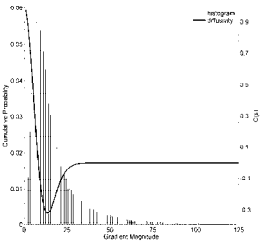

(n) The histogram of the original Lena image and diffusivity ($\gamma = 25$)

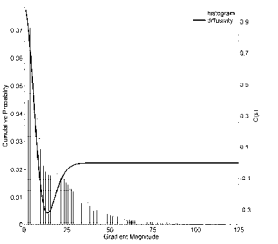

(o) The histogram of the filtered Lena image and diffusivity ($\gamma = 25$)

Fig. 15 Impact of γ on the TFAB diffusion method's performance (β=0.006, ξ=2).

(a) $\xi = 1$

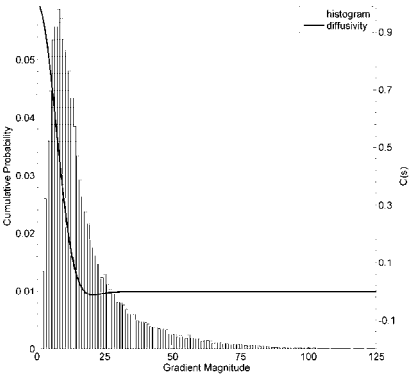

(b) The histogram of the original Lena image and diffusivity ($\xi = 1$)

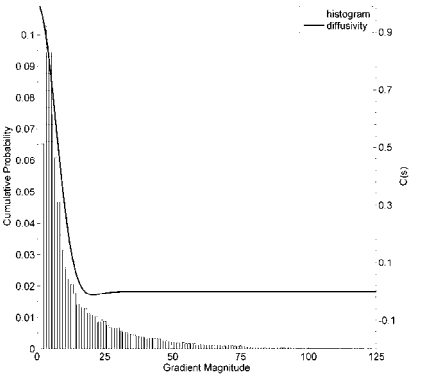

(c) The histogram of the filtered Lena image and diffusivity ($\xi = 1$)

(d) $\xi = 2$

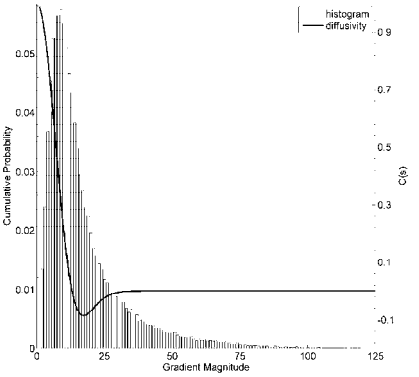

(e) The histogram of the original Lena image and diffusivity ($\xi = 2$)

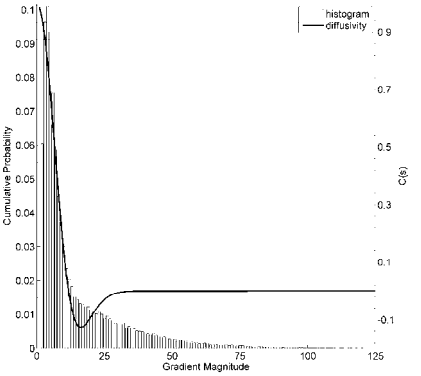

(f) The histogram of the filtered Lena image and diffusivity ($\xi = 2$)

(g) $\xi = 3$

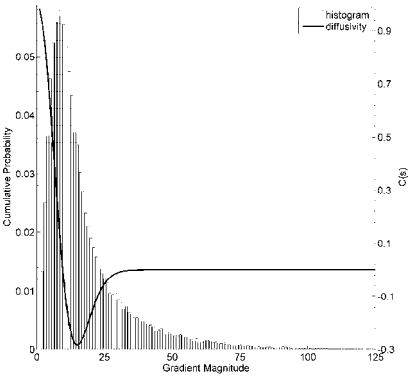

(h) The histogram of the original Lena image and diffusivity ($\xi = 3$)

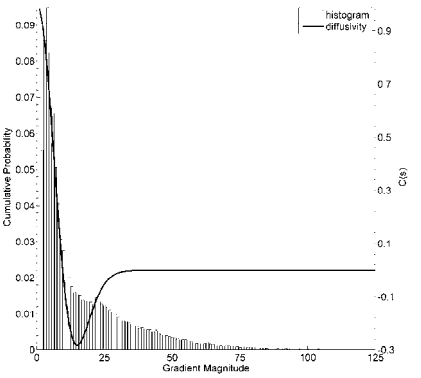

(i) The histogram of the filtered Lena image and diffusivity ($\xi = 3$)

Fig. 16 Impact of ξ on the TFAB diffusion method's performance (β=0.006, γ=8).

$$Q = \frac{1}{M}\sum_{M=1}^{j} Q_j, \tag{10}$$

where M is the total step number and Q_j denotes the local quality index computed within the moving window. In this paper, a sliding window of size 8×8 is applied to estimate an entire image. The list of PSNR and UIQI values that are reported by the different algorithms, which were performed on four blurred (σ=1) and noisy (σ^2=50) versions of test images used in our experiments, are found in Table 1. Remarkably, the statistical results shown in Table 1 definitely indicate that all three FAB diffusion algorithms are better than the existing anisotropic diffusion algorithms. Also, the

Table 4 PSNR and quality value for Lena image with different ξ.

Parameter	PSNR (dB)	UIQI
$\xi=1$	36.60	0.8081
$\xi=2$	36.72	0.8214
$\xi=3$	35.93	0.7954

better performance of the proposed TFAB diffusion is apparent.

3.2 *Impact of Parameters*

In Section 2.3, we provided detailed explanations on how the parameters in Eq. (8) can be used to tune the diffusion. In this section, we perform the three-dimensional analysis to evaluate the parameters' impact on the method's performance using the image of Lena. To this end, we apply the proposed algorithm to Fig. 12(b) using different settings of β for evaluation. The resultant images filtered by our method are shown in Figs. 14(a), 14(d), 14(g), 14(j), and 14(m), respectively. In Fig. 14, we believe that if β is too small, then the diffusion evolution results in deblurring fine details, such as the hat, its decoration and the hair [see Fig. 14(a)]. On the other hand, if β is too large, there are some oscillations in the face [see Figs. 14(j) and 14(m)]. In addition, we demonstrate the plots of original and enhanced image histograms and diffusivity in Figs. 14(b), 14(c), 14(e), 14(f), 14(h), 14(i), 14(k), 14(l), 14(n), and 14(o), respectively. From these plots, we can easily observe that β governs the range of gradient magnitudes to be enhanced during the evolution procedure [see the position of diffusivity as $c(s)<0$]. The list of PSNR and UIQI values by our algorithm with different settings of β are demonstrated in Table 2. We note from Table 3 that it is optimal for β to be in the range of 0.004–0.006. The more edge features the image contains, the larger β should be. On the contrary, the more smooth regions the image contains, the smaller β should be. Meanwhile, it is evident from image histograms that the gradient magnitudes become lower and lower during the diffusing process. As time advances, only smoother and smoother regions are being filtered, whereas large gradient magnitudes can be enhanced due to backward diffusion. It can be also concluded that we can perform empirical analysis to select the optimal set of parameters by comparing the original and resultant image histograms. We exhibit the impact of γ on our algorithm in Fig. 15 by enhancing the Lena image. It is obvious that γ controls the degree of inverse diffusion [see the degree of bending of diffusivity as $c(s)<0$]. The list of PSNR and UIQI values by our algorithm with different settings of γ are given in Table 3. Because inverse diffusion can easily cause noise amplification, which decreases the image quality, γ should

Table 6 Parameter settings of the proposed TFAB algorithm with respect to different noise variances.

Noise variance	Parameters
25	$\beta=0.01$, $\gamma=6$, $\xi=2$
50	$\beta=0.006$, $\gamma=8$, $\xi=2$
100	$\beta=0.004$, $\gamma=6$, $\xi=2$
225	$\beta=0.002$, $\gamma=8$, $\xi=2$
400	$\beta=0.001$, $\gamma=6$, $\xi=2$

Table 5 Performance [PSNR (dB) & UIQI] of the proposed TFAB algorithm for the images of Parrot, Lena, Cameraman, and Couple with respect to different noise variances.

		noise variance									
		25		50		100		225		400	
Scheme	Image	PSNR (dB)	UIQI	PSNR (dB)	UIQI	PSNR (dB)	UIQI	PSNR (dB)	UIQI	PSNR (dB)	UIQI
Blurred and noisy	Parrots	28.04	0.6188	27.07	0.5351	25.64	0.4458	23.36	0.3483	21.41	0.2794
	Lena	36.65	0.7661	34.98	0.6910	32.93	0.6024	30.10	0.4952	27.80	0.4092
	Cameraman	25.89	0.4506	25.29	0.4066	24.34	0.3646	22.62	0.3143	20.97	0.2764
	Couple	27.88	0.7427	26.97	0.6866	25.58	0.6165	23.30	0.5104	21.33	0.4289
TFAB	Parrots	28.63	0.7834	28.42	0.7514	28.14	0.7009	27.42	0.6534	27.08	0.6102
	Lena	37.46	0.8506	36.72	0.8214	35.96	0.7835	34.23	0.7100	33.20	0.6576
	Cameraman	26.21	0.5579	25.97	0.5224	25.73	0.4714	25.08	0.4118	24.82	0.3832
	Couple	28.29	0.7778	27.97	0.7556	27.56	0.7308	26.34	0.6491	25.90	0.6019

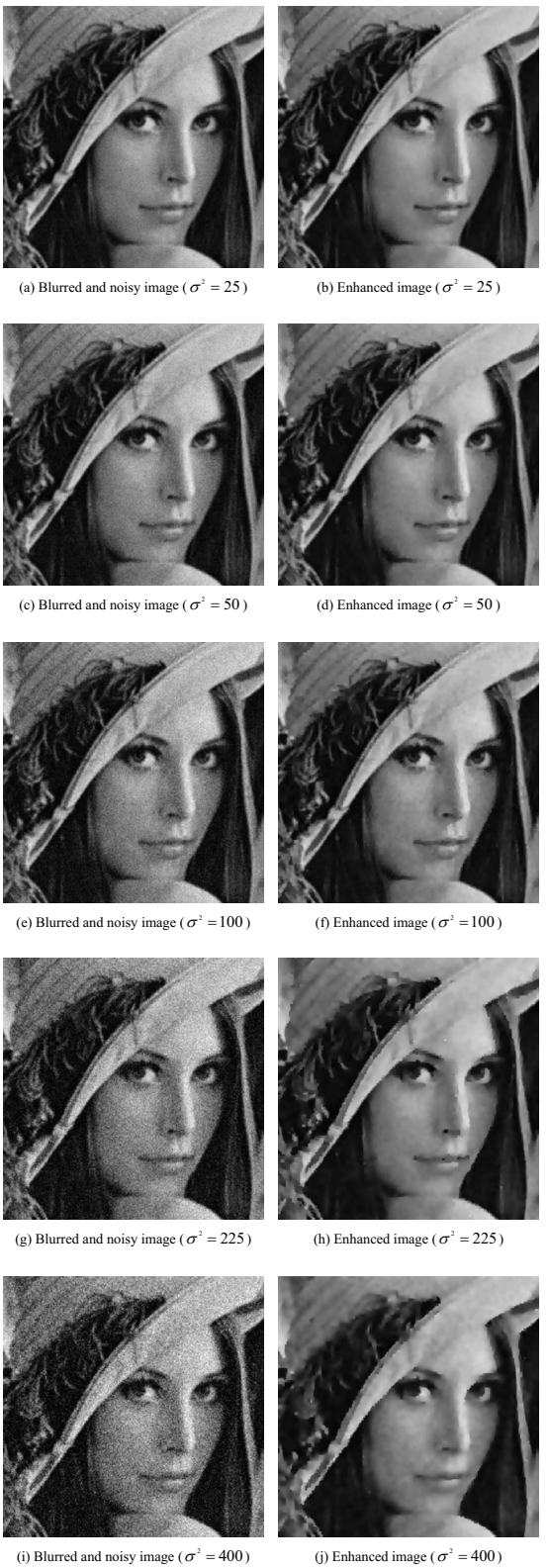

Fig. 17 Enhanced Gaussianly blurred Lena image (σ=1) using our algorithm with respect to different noise variances (10 iterations).

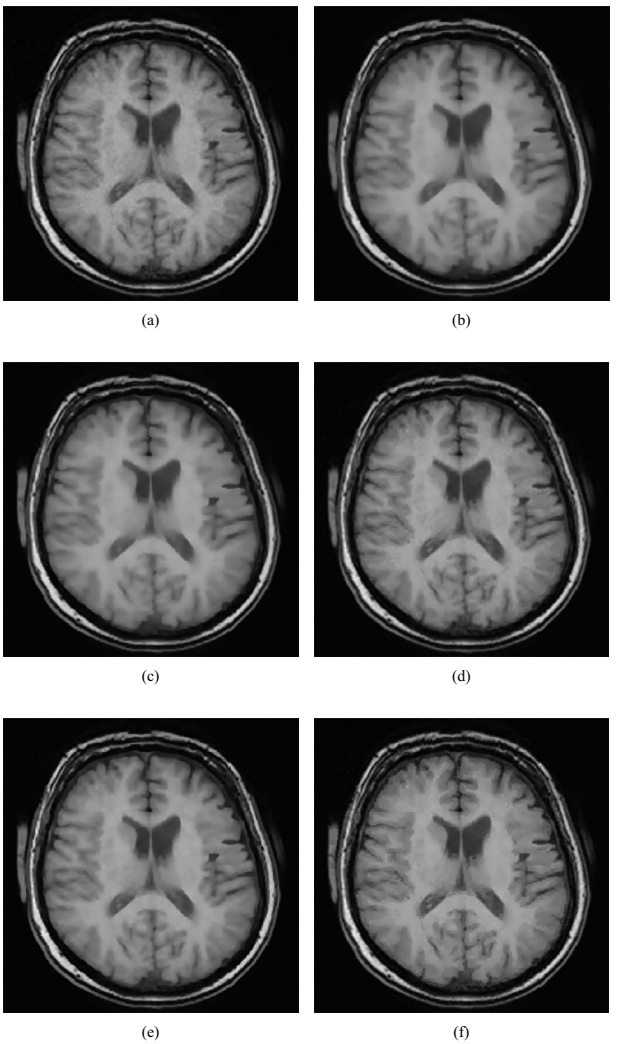

Fig. 18 Comparison of the five diffusion methods using a MR image: (a) Brain MR image; (b–f) filtered images corresponding to the image in (a) resulting from CLMC anisotropic diffusion (ρ=0.05), MB anisotropic diffusion (ρ=0.05), GSZ FAB diffusion (k_f=0.25∗MAG, k_b=2∗MAG, α=0.25), LVCFAB diffusion (k_f=50, k_b=200, β_1=0.1, β_2=0.02, ρ=0.25, α=0.5), and the proposed TFAB diffusion (β =0.006, γ=8, ξ=4) (10 iterations).

not be fixed too large. In our experiments, we suggest that γ be selected within the bound: $\gamma \leqslant 15$. As mentioned in Section 2.3, ξ determines the ratio between forward diffusion and backward diffusion. Thus, it is significant to explore the impact of ξ on our method. The resultant images are illustrated in Fig. 16 by modulating ξ while fixing β and γ in the proposed algorithm. It is clear that if ξ is too small, then our method evolves as a traditional anisotropic diffusion process and results in an imperceptible enhancement effect [see Fig. 16(a)]. On the contrary, if ξ is too large, our method is highly unstable and often leads to noise amplification [see Fig. 16(g)]. The statistical results in Table 4 confirm that ξ should be carefully selected. Our simulations on various images including those not reported here, confirm that the parameter should be in the range of 1–3, so that it can guarantee the realization of the tunable FAB diffusion instead of the classic anisotropic diffusion or inverse diffusion.

The aim of this paper is to present a TFAB diffusion algorithm and to apply it in image enhancement as well as image sharpening. We focus on enhancing and sharpening blurry signals, while still allowing some additive noise to

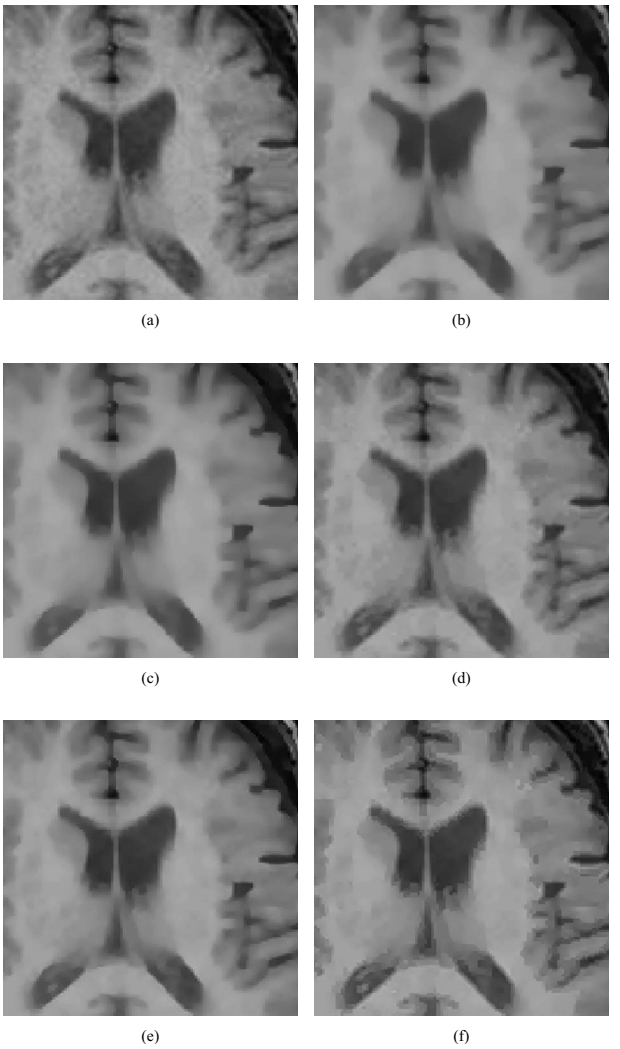

Fig. 19 A regional enlarged portion of interest of original image and results corresponding to Fig. 18(c)–18(g).

interfere with the process. To demonstrate the effectiveness of the proposed TFAB algorithm in noise reduction, the PSNR and UIQI values of the original and enhanced images for our algorithm with respect to different noise variances are listed in Table 5. In addition, the parameter settings of the proposed algorithm at different noise levels are listed in Table 6. From the PSNR and UIQI values, we can see that the proposed TFAB algorithm can effectively achieve noise reduction and greatly improve image quality. To compare the visual quality of the result from our algorithm, its enhanced images with respect to different noise variances are shown in Fig. 17. By comparing the noisy image and enhanced image at different noise levels, we can see that sharpening and denoising can be reconciled by the proposed tunable mechanism that controls the orientation, type, and extent of the diffusion process. Meanwhile, it is obvious from Table 6 that β is sensitive to noise levels and should be lower as noise variance increases.

3.3 *Medical Images*

In medical images, low SNR and CNR often degrade the information and affect several image-processing tasks, such as segmentation, classification, and registration. Therefore, it is of considerable interest to improve SNR and CNR to reduce the deterioration of image information. In this section, we present an example from magnetic resonance (MR) patient studies.

We present in Fig. 18 an example of the performance of the different diffusion algorithms for MR image enhancing. The original MR image is depicted in Fig. 18(a) with the size of 256×256. The results for the five algorithms are shown in Figs. 18(b)–18(f). As seen from all five enhanced images, the smoothness in homogeneous regions, such as white matter, seems to be visually the same in all images, while the TFAB diffusion algorithm achieves greater contrast and produces more reliable edges, which is especially useful for segmentation and classification purposes necessary in medical image applications.

Figure 19 shows a regional enlarged portion of interest from Fig. 18(a) and the diffusive filtered results of this portion using the five diffusion algorithms. As expected, the five algorithms remove noise present in Fig. 19(a) and simultaneously smooth the homogeneous regions. According to the visual analyses of the image quality, the results generated by the three FAB diffusion processes are comparable. However, the boundary contrast appears to be higher using the proposed TFAB algorithm when compared to other algorithms. In addition, the TFAB diffusion enhances boundary sharpness and fine structures better than other diffusion methods.

4 Conclusion

Digital image acquisition techniques often suffer from low SNR and CNR, which degrade the information contained in the digital image and thus reduce its potential utility for industry use. We have presented a novel TFAB diffusion algorithm for image restoration and enhancement to improve on the SNR and CNR that preclude the current utility of digital images for industry. The primary advantage of the proposed diffusion algorithm is that tenability of the improved diffusion coefficient offers user flexibility to adjust edge-enhancing performance. At the same time, it is not necessary to consider the rational time-consuming strategy for estimating the gradient threshold. The proposed algorithm was tested on various digital images, including four general images and a medical image. The results from our simulations show an improvement in visual effect and quantitative analyses over the preexisting algorithms.

Acknowledgments

This work was supported, in part, by the following: the National High Technology R&D (863) Program of China under Grant 2007AA12Z160; National Natural Science Foundation of China under Grants No. 40901205, No. 40771139, and No. 40930532, Foundation of the State Key Laboratory of Information Engineering in Surveying, Mapping and Remote Sensing under Grant No. 08R02, Foundation of Key Laboratory of Mapping from Space of State Bureau of Surveying and Mapping under Grant No. 200809, Key Laboratory of Mine Spatial Information Technologies (Henan Polytechnic University, Henan Bureau of Surveying and Mapping), State Bureau of Surveying and Mapping, and the Special Fund for Basic Scientific Research of Central Colleges, China University of Geo-

sciences, Wuhan, under Grant No. GUGL090210. The authors would also like to thank the anonymous reviewers for their valuable comments and suggestions which significantly improved the quality of this paper.

References

1. N. Damera-Venkata, T. D. Kite, W. S. Geisler, B. L. Evans, and A. C. Bovik, "Image quality assessment based on a degradation model," *IEEE Trans. Image Process.* **9**(4), 636–650 (2000).
2. J. S. Lee, "Digital image enhancement and noise filtering by use of local statistics," *IEEE Trans. Pattern Anal. Mach. Intell.* **PAMI-2**, 165–168 (1980).
3. P. Chan and J. Lim, "One-dimensional processing for adaptive image restoration," *IEEE Trans. Acoust., Speech, Signal Process.* **33**(1), 117–126 (1985).
4. D. C. C. Wang, A. H. Vagnucci, and C. C. Li, "Gradient inverse weighted smoothing scheme and the evaluation of its performance," *Comput. Graph. Image Process.* **15**(2), 167–181 (1981).
5. K. Rank and R. Unbehauen, "An adaptive recursive 2-D filter for removal of Gaussian noise in images," *IEEE Trans. Image Process.* **1**(3), 431–436 (1992).
6. C. B. Ahn, Y. C. Song, and D. J. Park, "Adaptive template filtering for signal-to-noise ratio enhancement in magnetic resonance imaging," *IEEE Trans. Med. Imaging* **18**(6), 549–556 (1999).
7. S. M. Smith and J. M. Brady, "SUSAN—a new approach to low level image processing," *Int. J. Comput. Vis.* **23**(1), 45–78 (1997).
8. T. Iijima, "Basic theory of pattern observation," *Papers of Technical Group on Automata and Automatic Control*, IECE, Japan (1959) (in Japanese).
9. T. Iijima, "Basic theory on normalization of a pattern (in case of typical one-dimensional pattern)," *Bull. Elec. Lab.* **26**, 368–388 (1962).
10. J. Weickert, S. Ishikawa, and A. Imiya, "Linear scale-space has first been proposed in Japan," *J. Math. Imaging Vision* **10**(3), 237–252 (1999).
11. A. P. Witkin, "Scale-space filtering," in *Proc. of Int. Joint Conf. on Artificial Intelligence*, ACM, New York, pp. 1019–1021 (1983).
12. J. J. Koenderink, "The structure of images," *Biol. Cybern.* **50**, 363–370 (1984).
13. J. J. Koenderink and A. J. V. Doorn, "Generic neighborhood operators," *IEEE Trans. Pattern Anal. Mach. Intell.* **14**(6), 597–605 (1992).
14. T. Lindeberg, "Feature detection with automatic scale selection," *Int. J. Comput. Vis.* **30**(2), 77–116 (1998).
15. A. L. Yuille and T. Poggio, "Scaling theorems for zero-crossings," *IEEE Trans. Pattern Anal. Mach. Intell.* **8**(1), 15–25 (1986).
16. J. Babaud, A. P. Witkin, M. Baudin, and R. O. Duda, "Uniqueness of the Gaussian kernel for scale-space filtering," *IEEE Trans. Pattern Anal. Mach. Intell.* **8**(1), 26–33 (1986).
17. P. Perona and J. Malik, "Scale-space and edge detection using anisotropic diffusion," *IEEE Trans. Pattern Anal. Mach. Intell.* **12**(7), 629–639 (1990).
18. F. Catte, P. L. Lions, J. M. Morel, and T. Coll, "Image selective smoothing and edge detection by nonlinear diffusion," *SIAM (Soc. Ind. Appl. Math.) J. Numer. Anal.* **29**(1), 182–193 (1992).
19. L. Alvarez, P. L. Lions, and J. M. Morel, "Image selective smoothing and edge detection by nonlinear diffusion," *SIAM (Soc. Ind. Appl. Math.) J. Numer. Anal.* **29**(3), 845–866 (1992).
20. L. Alvarez and L. Mazzora, "Signal and image restoration using shock filters and anisotropic diffusion," *SIAM (Soc. Ind. Appl. Math.) J. Numer. Anal.* **31**, 590–605 (1994).
21. G. Gerig, O. Kubler, R. Kikinis, and F. A. Jolesz, "Nonlinear anisotropic filtering of MRI data," *IEEE Trans. Med. Imaging* **11**(2), 221–232 (1992).
22. R. T. Whitaker and S. M. Pizer, "A multi-scale approach to nonuniform diffusion," *Comput. Vis. Graph. Image Process.* **57**, 99–110 (1993).
23. X. Li and T. Chen, "Nonlinear diffusion with multiple edginess thresholds," *Pattern Recogn.* **27**(8), 1029–1037 (1994).
24. S. T. Acton, "Multigrid anisotropic diffusion," *IEEE Trans. Image Process.* **7**(3), 280–291 (1998).
25. S. T. Acton, "Locally monotonic diffusion," *IEEE Trans. Signal Process.* **48**(5), 1379–1389 (2000).
26. J. Weickert, "Theoretical foundations of anisotropic diffusion in image processing," *Computing* **11**, 221–236 (1996).
27. J. Weickert, B. M. T. H. Romeny, and M. A. Viergever, "Efficient and reliable schemes for nonlinear diffusion filtering," *IEEE Trans. Image Process.* **7**(3), 398–410 (1998).
28. J. Weickert, "Applications of nonlinear diffusion in image processing and computer vision," *Acta Math. Univ. Comen.* **70**(1), 33–50 (2001).
29. Y. Yu-Li, X. Wenyuan, A. Tannenbaum, and M. Kaveh, "Behavioral analysis of anisotropic diffusion in image processing," *IEEE Trans. Image Process.* **5**(11), 1539–1553 (1996).
30. B. Fischl and E. L. Schwartz, "Adaptive nonlocal filtering: a fast alternative to anisotropic diffusion for image enhancement," *IEEE Trans. Pattern Anal. Mach. Intell.* **21**(1), 42–48 (1999).
31. M. J. Black, G. Sapiro, D. H. Marimont, and D. Heeger, "Robust anisotropic diffusion," *IEEE Trans. Image Process.* **7**(3), 421–432 (1998).
32. G. Gilboa, N. Sochen, and Y. Y. Zeevi, "Forward-and-backward diffusion processes for adaptive image enhancement and denoising," *IEEE Trans. Image Process.* **11**(7), 689–703 (2002).
33. P. K. Saha and J. K. Udupa, "Scale-based diffusive image filtering preserving boundary sharpness and fine structures," *IEEE Trans. Med. Imaging* **20**(11), 1140–1155 (2001).
34. F. Voci, S. Eiho, N. Sugimoto, and H. Sekibuchi, "Estimating the gradient in the Perona-Malik equation," *IEEE Signal Process. Mag.* **21**(3), 39–65 (2004).
35. H. Yu and C. S. Chua, "GVF-based anisotropic diffusion models," *IEEE Trans. Image Process.* **15**(6), 1517–1524 (2006).
36. Y. Yue, M. M. Croitoru, A. Bidani, J. B. Zwischenberger, and J. W. Clark, "Nonlinear multiscale wavelet diffusion for speckle suppression and edge enhancement in ultrasound images," *IEEE Trans. Med. Imaging* **25**(3), 297–311 (2006).
37. K. Karl, W. Carl-Fredrik, K. Ron, and G. V. Kirby, "Oriented speckle reducing anisotropic diffusion," *IEEE Trans. Image Process.* **16**(5), 1412–1424 (2007).
38. J. Martin-Herrero, "Anisotropic diffusion in the hypercube," *IEEE Trans. Geosci. Remote Sens.* **45**(5), 1386–1398 (2007).
39. Y. Wang, L. Zhang, and P. Li, "Local varianced-controlled forward-and-backward diffusion for image enhancement and noise reduction," *IEEE Trans. Image Process.* **16**(7), 1854–1864 (2007).
40. B. Smolka and K. N. Plataniotis, "On the coupled forward and backward anisotropic diffusion scheme for color image enhancement," in *Lecture Notes in Computer Science*, pp. 70–80, Springer, New York (2002).
41. G. Gilboa, N. Sochen, and Y. Y. Zeevi, "Image sharpening by flows based on triple well potentials," *J. Math. Imaging Vision* **20**(1), 121–131 (2004).
42. M. Welk, G. Gilboa, and J. Weickert, "Theoretical foundations for discrete forward-and-backward diffusion filtering," in *Lecture Notes in Computer Science*, pp. 527–538, Springer, New York (2009).
43. G. Aubert and P. Kornprobst, *Mathematical Problems in Image Processing: Partial Differential Equations and The Calculus of Variations*, Springer-Verlag, Berlin (2002).
44. G. Aubert and L. Vese, "A variational method in image recovery," *SIAM (Soc. Ind. Appl. Math.) J. Numer. Anal.* **34**(5), 1948–1979 (1997).
45. J. Weickert, *Anisotropic Diffusion in Image Processing*, BG Teubner, Stuttgart (1998).
46. R. C. Gonzalez and R. E. Woods, *Digital Image Processing*, Prentice Hall, Englewood Cliffs, NJ (2002).
47. J. Monteil and A. Beghdadi, "A new interpretation of the nonlinear anisotropic diffusion for image enhancement," *IEEE Trans. Pattern Anal. Mach. Intell.* **21**(9), 940–946 (1999).
48. G. Gilboa, Y. Y. Zeevi, and N. Sochen, "Image enhancement segmentation and denoising by time dependent nonlinear diffusion processes," in *Proc. of IEEE Int. Conf. on Image Processing* (ICIP '01), Thessaloniki, Greece, pp. 134–137 (2001).
49. P. Mrázek and M. Navara, "Selection of optimal stopping time for nonlinear diffusion filtering," *Int. J. Comput. Vis.* **52**(2/3), 189–203 (2003).
50. Z. Wang and A. C. Bovik, "A universal image quality index," *IEEE Signal Process. Lett.* **9**(3), 81–84 (2002).

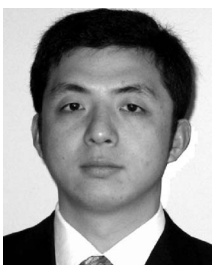

Yi Wang received his BS, MS, and PhD in photogrammetry and remote sensing from Wuhan University, Wuhan, in 2002, 2004, and 2007, respectively. He is currently an associate professor with the Institute of Geophysics and Geomatics, China University of Geosciences. His research interests include remote sensing image processing using partial differential equations, and particularly, pattern recognition.

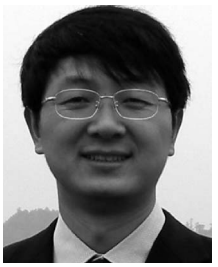

Ruiqing Niu received his BS, MS, and PhD from China University of Geosciences, Wuhan, in 1992, 2001, 2005, respectively. He is currently an associate professor with the Institute of Geophysics and Geomatics, China University of Geosciences. His research interests include geovisualization, environmental remote sensing, and geological remote sensing.

Xin Yu received his PhD in pattern recognition and intelligent system from Huazhong University of Science and Technology, Wuhan, China, in 2007. He is currently a Lecturer with the Institute of Geography and Geomatics, China University of Geosciences. His research interests include computer vision, pattern recognition, and their applications in remote sensing and geology.

Liangpei Zhang received his BS in physics from Hunan Normal University, Changsha, China, in 1982, MS in optics from the Xi'an Institute of Optics and Precision Mechanics of the Chinese Academy of Sciences, Xi'an, in 1988, and PhD in photogrammetry and remote sensing from Wuhan University, Wuhan, China, in 1998. From 1997 to 2000, he was a professor with the School of the Land Sciences, Wuhan University. In August 2000, he joined the State Key Laboratory of Information Engineering in Surveying, Mapping, and Remote Sensing, Wuhan University, as a professor and head of the Remote Sensing Section. He has published more than 120 technical papers. His research interests include hyperspectral remote sensing, high-resolution remote sensing, image processing, and artificial intelligence. Dr. Zhang has served as co-chair of the SPIE Series Conferences on Multispectral Image Processing and Pattern Recognition (MIPPR) and the Conference on Asia Remote Sensing in 1999; editor of the MIPPR01, MIPPR05, Geoinformatics Symposiums; associate editor of the *Geo-spatial Information Science Journal*; on the Chinese National Committee for the International Geosphere-Biosphere Programme; and as executive member for the China Society of Image and Graphics.

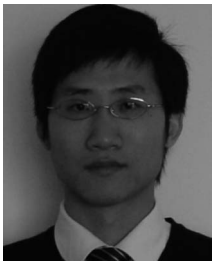

Huanfeng Shen received his BS, MS, and PhD in photogrammetry and remote sensing from Wuhan University, Wuhan, in 2002, 2004, and 2007, respectively. He is currently an associate professor at the School of Resource and Environmental Science, Wuhan University. His main research interest is image superresolution enhancement.